ADVANCED QUANTUM TECHNOLOGIES
www.advquantumtech.com

Manipulation of the Magnetoresistance by Strain in Topological $TaSe_3$

*Jie Xing, Joanna Blawat, Smita Speer, Ahmad Ikhwan Us Saleheen, John Singleton, and Rongying Jin**

1D $TaSe_3$ exhibits many unusual physical properties due to its distorted type-II chains. Ribbon-shaped single crystals can be easily bended along the *b*-axis, forming rings. This study investigates the magnetoresistance (MR) of $TaSe_3$ up to 60 T in both unbended (ribbon shape) and ring-shaped (bended ribbon) samples. Notable changes are found in the magnetotransport properties between the two different shaped samples. One is that the MR in ring-shaped samples is three orders lower than that in unbended samples under the same sample environment. In addition, linear MR is observed above ≈20 T in ring-shaped samples when the magnetic field is parallel or perpendicular to the rings. Quantum oscillations are also observed as a function of the magnetic field when the magnetic field is applied parallel to rings, possibly due to the Altshuler–Aronov–Spivak effect or the inversion of the lowest Landau level beyond the quantum limit. All these results are related to strain-induced electronic structure change in $TaSe_3$, an effective way to tune physical properties in low-dimensional materials.

1. Introduction

Topological materials have attracted much interest due to their nontrivial topological properties and novel phenomena, such as extremely large magnetoresistance and topological superconductivity.[1–6] A topological superconductor hosts Majorana bound states or Majorana fermions, which has potential applications in topological quantum computation.[7] Quasi-1D compound $TaSe_3$ has been found to exhibit superconductivity below 2.3 K with a semimetallic normal state.[8–10] Unlike other transition-metal trichalcogenides, there is no charge density wave transition in $TaSe_3$.[11,12] First-principles calculations suggest the nontrivial topological phases caused by the distorted type-II chain in $TaSe_3$.[13,14] The results reveal strong 3D topological insulating (TI) character with the Dirac states on the surface. By applying strains along the *a*- and/or *c*-axis, multiple topological phases, such as strong/weak TI and Dirac semimetal, could be realized.[14] Recent experiments and calculations also confirm a topological phase transition by applying strain along the *b*-axis.[15]

Strain effect on $TaSe_3$ has been studied by bending ribbon crystals into a ring shape.[16–19] Bending creates nonuniform strain along the *b*-axis of $TaSe_3$ and induces the deformation energy, thus generating defects/disorder in a crystal for relaxation.[20] Cylindrical domain walls from the edge dislocations and vortex have been suggested in ring-shaped crystals.[17] Given the observed nontrivial topological band and extremely large magnetoresistance (XMR) in as-grown ribbon-shaped samples[21–23] and a uniform strain-induced topological phase transition,[15] we are inspired to investigate the magnetotransport properties in ring-shaped $TaSe_3$ single crystals by applying magnetic field up to 60 T. Compared to as-grown unbended samples, the MR in ring-shaped samples reduces three orders of magnitude. Furthermore, we find change in field dependence from a quadratic behavior below ≈10 T to a linear field dependence above 20 T in both H ⊥ ring and H // ring configurations. For H // ring, the MR also oscillates with the applied magnetic field with the period proportional to H, different from Shubnikov–de Haas (SdH) type oscillation. Possible origin for such oscillation is discussed.

2. Results and Discussion

Single crystals of $TaSe_3$ were synthesized by the chemical vapor transport method.[22] The electrical resistivity was measured using the standard four-probe method for unbended (as-grown)

J. Xing, J. Blawat, A. I. U. Saleheen, R. Jin
Center for Experimental Nanoscale Physics, Department of Physics and Astronomy
University of South Carolina
Columbia, SC 29208, USA
E-mail: rjin@mailbox.sc.edu

J. Blawat, S. Speer, R. Jin
Department of Physics and Astronomy
Louisiana State University
Baton Rouge, LA 70803, USA

J. Singleton
National High Magnetic Field Laboratory
Los Alamos National Laboratory
Los Alamos, NM 87545, USA

The ORCID identification number(s) for the author(s) of this article can be found under https://doi.org/10.1002/qute.202200094

© 2022 The Authors. Advanced Quantum Technologies published by Wiley-VCH GmbH. This is an open access article under the terms of the Creative Commons Attribution-NonCommercial-NoDerivs License, which permits use and distribution in any medium, provided the original work is properly cited, the use is non-commercial and no modifications or adaptations are made.

DOI: 10.1002/qute.202200094

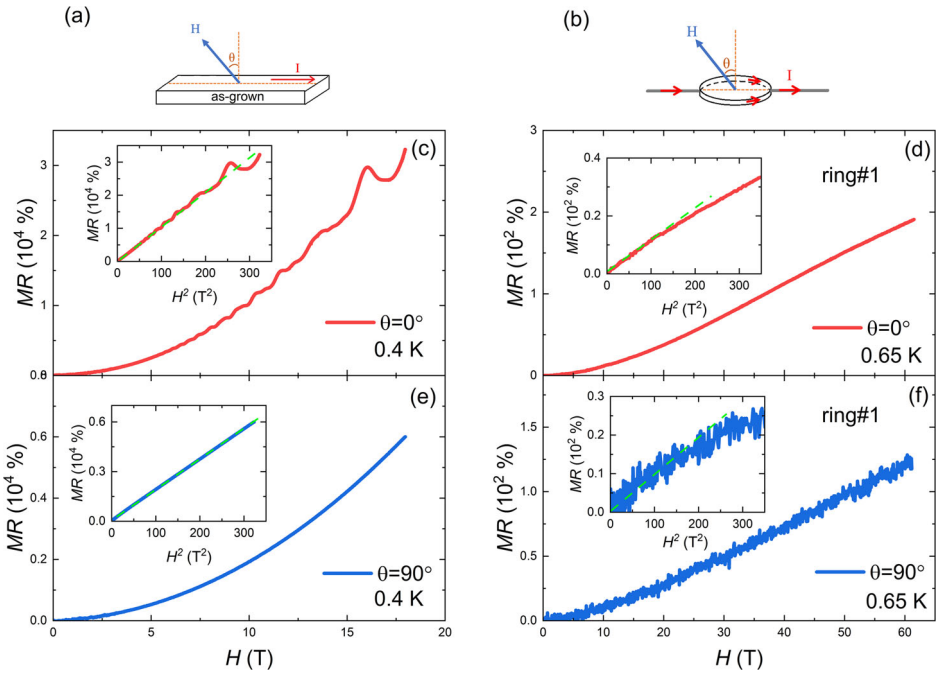

Figure 1. a,b) Sketches of an unbended ribbon sample and a ring-shaped sample. c) MR versus magnetic field for a ribbon-shaped sample at 0.65 K with $\theta = 0°$. Inset: MR data plotted as a function of H^2 (red) and a linear fit (green). d) MR versus magnetic field for ring #1 at 0.65 K with $\theta = 0°$. Inset: MR data plotted as a function of H^2 (red) and a linear fit at low fields (green). e) MR versus magnetic field for a ribbon-shaped sample at 0.65 K with $\theta = 90°$. Inset: MR data plotted as a function of H^2 (blue) and a linear fit (green). f) MR versus magnetic field for ring #1 at 0.65 K with $\theta = 90°$. Inset: MR data plotted as a function of H^2 (red) and a linear fit at low fields (green).

and ring-shaped samples in a Physical Property Measurement System with 14 T DC field (PPMS-14 T, *Quantum Design*) and a SCM2 He-3 system with 18 T DC field at the National High Magnetic Field Laboratory. The ring-shaped samples were prepared by bending ribbon crystals, as shown in **Figure 1**b. The ring area and thickness are 0.42 mm^2 (with a diameter ≈ 0.73 mm) and 0.05 mm for ring #1, 1.76 mm^2 (with a diameter ≈ 1.5 mm) and 0.25 mm for ring #2. The magnetoresistance measured up to 60 T was performed in a pulse field at National High Magnetic Field Laboratory, Los Alamos.

Figure 1a,b shows the magnetic field (H) and current (I) configurations for both as-grown ribbon (unbended) and ring-shaped samples, respectively. At $\theta = 0°$, H is normal to the ribbon or ring. At $\theta \approx 90°$, H // I in the ribbon sample or in the ring plane. The MR is calculated using the formula $MR = \frac{\rho(T,H)-\rho(T,0)}{\rho(T,0)}$ at variable temperatures and magnetic fields. Figure 1c–f presents the magnetic field dependence of MR for the ribbon (Figure 1c,e) and ring-shaped (Figure 1d,f) samples at indicated temperatures at $\theta = 0°$ and 90°, respectively. Measurements were performed at 0.4 K for the ribbon sample and 0.65 K for the ring-shaped sample (ring #1), neither showing any sign of superconductivity. As shown in ref. [22], the residual resistivity ratio of our single crystals exceeds that in the literature.[9–11] The absence of superconductivity in our crystals is not related to the sample quality. In terms of MR, the obvious difference between two configurations can be clearly seen. First, MR(ring) ≪ MR(ribbon) for both $\theta = 0°$ and 90° under the same field. Second, as demonstrated in the insets of Figure 1c,e, MR(ribbon) exhibits straight H^2 behavior up to 18 T, while MR(ring) deviates from the H^2 dependence above ≈10 T for both $\theta = 0°$ and 90° (see the insets of Figure 1c–f). Above 10 T, MR(ring) gradually changes from low-field behavior to linear H dependence above ≈20 T. These indicate that the scattering in the ring-shaped samples is severely modified compared to the ribbon case.

The suppression of the MR by pressure has been observed in WTe_2 due to the imperfect balance between electron and hole pockets by pressure-induced Fermi energy change.[24] The absence of the SdH oscillations in MR(ring) of $TaSe_3$ up to 60 T (Figure 1d,f) strongly suggests the modification of the Fermi surface in the ring-shaped sample compared to the ribbon case (Figure 1c,e). According to theoretical calculations, strain along the *a*, *b*, and *c*-axes could tune the band structure near the Fermi surface of $TaSe_3$.[13,15] Since the ring-shaped samples are prepared by bending single crystals, the strain may be induced most likely along the *b*-axis. If the large MR in unbended ribbon $TaSe_3$ results from electron–hole compensation,[22] bending the crystals leads to the reduced MR due to increased imbalance between electron and hole bands.

Figure 2 shows the field dependence of MR at different temperatures for H ⊥ ring ($\theta = 0°$) for ring #1 (a) and ring #2 (b), respectively. Note that MR(ring #1) > MR(ring #2), which is likely due to inhomogeneous strain distribution in ring #1 with a smaller diameter compared to ring #2. The overall temperature and field dependence of MR(ring #1) and MR(ring #2) are similar, i.e., they increase almost linearly with H above ≈20 T at a fixed temperature, and decrease with increasing temperature at a fixed field. As the as-grown ribbon sample shows nearly perfect Kohler's scaling behavior ($MR = \alpha(H/\rho_0)^n$, α is a constant and ρ_0 is the zero-field resistivity) with the exponent $n \approx 2$,[22] we also replot MR(ring #1) and MR(ring #2) as a function of H/R_0 (R_0 is the zero-field

© 2022 The Authors. Advanced Quantum Technologies published by Wiley-VCH GmbH

25119044, 2022, 12, Downloaded from https://onlinelibrary.wiley.com/doi/10.1002/qute.202200094 by Florida State University, Wiley Online Library on [31/05/2023]. See the Terms and Conditions (https://onlinelibrary.wiley.com/terms-and-conditions) on Wiley Online Library for rules of use; OA articles are governed by the applicable Creative Commons License

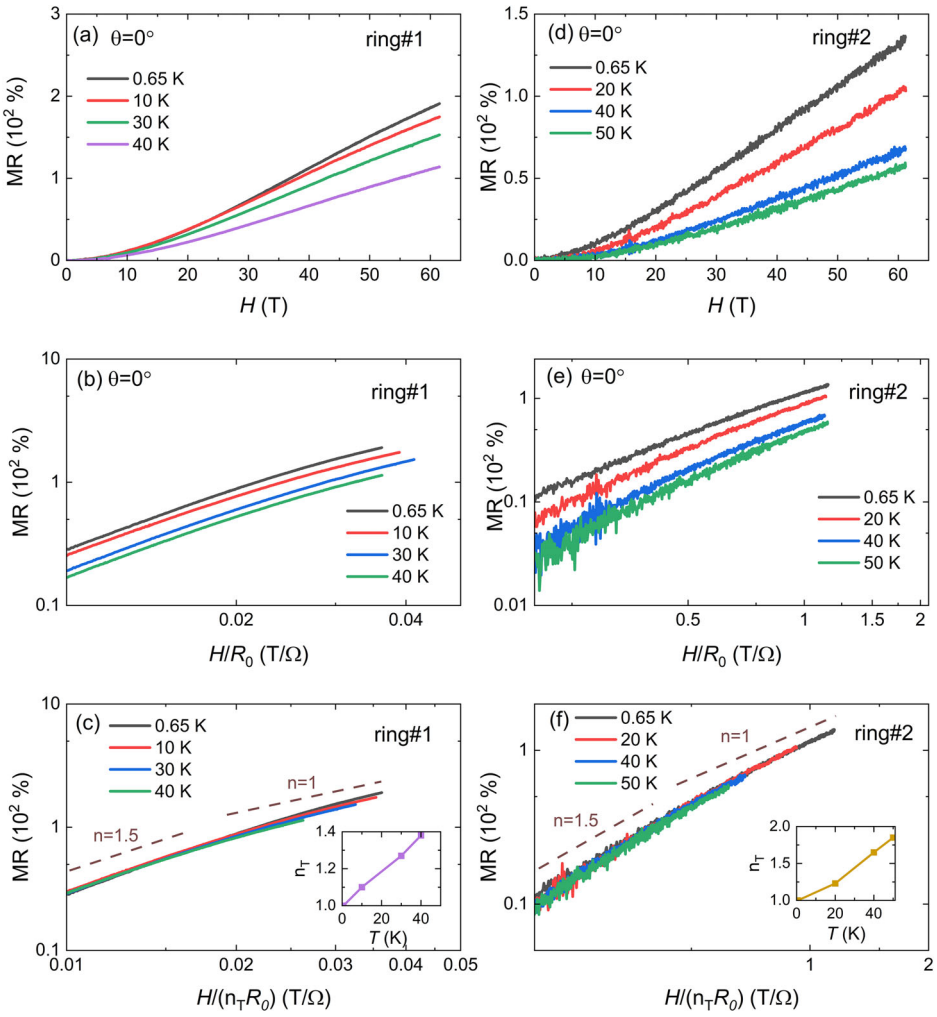

Figure 2. a,b) MR versus magnetic field at indicated temperatures for ring #1 and ring #2 at $\theta = 0°$; c,d) Kohler's plot of MR(ring #1) and MR(ring #2) at $\theta = 0°$; e,f) MR versus $H/(n_T R_0)$ for ring #1 and ring #2 at $\theta = 0°$.

resistance) in Figure 2c,d, respectively. For both rings, MR obtained at different temperatures does not collapse into a single curve, indicating the violation of the Kohler's rule. This further suggests the imbalance between electron and hole bands induced by crystal bending.

The violation of the Kohler's rule is also observed in a Weyl semimetal TaP, where an extended Kohler's rule is proposed with a temperature-dependent factor n_T.[25] Using the same method, we find that both MR(ring #1) and MR(ring #2) at different temperatures collapse into a single curve when plotted as a function of $H/(n_T R_0)$ as shown in Figure 2e,f, respectively. As demonstrated in the insets of Figure 2e,f, n_T increases with increasing temperature with more or less a linear fashion in both rings. Quantitatively, we can still fit MR(ring) = $[H/(n_T R_0)]^n$ with $n \approx 1.5$ at low fields and ≈1.0 above 20 T for both MR(ring #1) and MR(ring #2). The temperature-dependent n_T and $n \neq 2$ clearly indicate the modification of the electronic properties by crystal bending.

In the classic framework, the transverse MR (H ⊥ I) at the low magnetic field limit with $\omega_c \tau \ll 2\pi$ (ω_c is the cyclotron frequency and τ is the relaxation time) should follow the quadratic law with the magnetic field. If the magnetic field increases and crosses the high field limit with $\omega_c \tau \gg 2\pi$, the MR may turn to the linear field dependence which can be both intrinsic or extrinsic. Intrinsically, small Fermi surface pockets with small effective masses can give rise to the linear MR.[26–28] From our previous study, two experimentally probed bands from unbended $TaSe_3$ are not small.[22] Of course, bending could modify the band structure for the ring-shaped samples as discussed above. Given that it persists at higher temperatures, the linear MR may not be associated with Umklapp scattering[29] but related to disorders or defects induced by bending in our ring-shaped $TaSe_3$.[30,31]

Figure 3a,b shows the magnetic field dependence of MR(ring #1) and MR(ring #2) at $\theta = 90°$ in the temperature range between 0.65 and 50 K, respectively. Overall, the behavior of MR at $\theta = 90°$ is similar to the case of $\theta = 0°$ with a slightly smaller magnitude at the same temperature and field. The unique feature of MR(ring, $\theta = 90°$) is its oscillations in high fields. The oscillations are more profound with decreasing temperature in the ring #2 sample. Note these oscillations reveal different characteristic from the SdH oscillations seen in the unbended samples (Figure 1a): the period is proportional to H. In Figure 3c,d,

© 2022 The Authors. Advanced Quantum Technologies published by Wiley-VCH GmbH

25139044, 2022, 12, Downloaded from https://onlinelibrary.wiley.com/doi/10.1002/qute.202200094 by Florida State University, Wiley Online Library on [31/05/2023]. See the Terms and Conditions (https://onlinelibrary.wiley.com/terms-and-conditions) on Wiley Online Library for rules of use; OA articles are governed by the applicable Creative Commons License

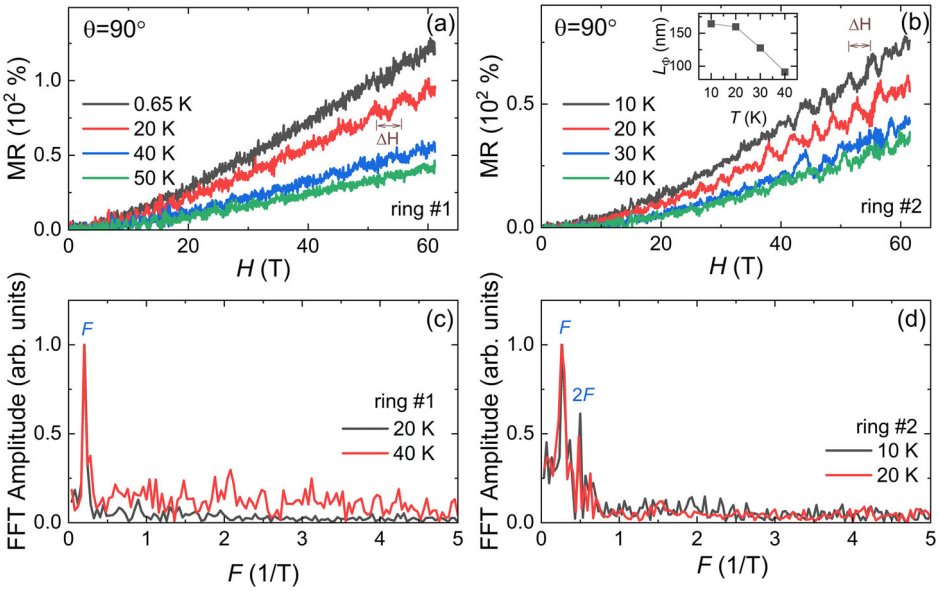

Figure 3. a,b) MR versus magnetic field at indicated temperatures for ring #1 and ring #2 at $\theta = 90°$. c,d) FFT spectra of the oscillations for ring #1 and ring #2, respectively.

we present the fast Fourier transform (FFT) spectra of the oscillations for ring #1 and ring #2, respectively. The period is ≈4.15 and ≈3.75 T at 20 K for ring #1 and ring #2, respectively. While there is only one major peak for the case of ring #1 (Figure 3c), the second harmonic frequency is clearly revealed in ring #2 (Figure 3d). There are three situations that can lead to linear-field oscillations. 1) Aharonov–Bohm (AB) oscillation[32] involves two carrier beams each travelling half loops and forming quantum interference when they meet. The period is $\Delta H = (h/e)/S$, where h is the Planck's constant, e is the electron charge, and S is the loop area that charge carriers encircled. 2) Altshuler–Aronov–Spivak (AAS) oscillation[33] is due to carriers travelling a whole loop surrounding a scattering center, thus forming quantum interference. The period is $\Delta H = (h/2e)/S$. 3) Quantum oscillation is due to the inversion of the lowest Landau level beyond the quantum limit.[34] The period is determined by both Fermi velocity and the g factor.

For the AB-type oscillation, H ⊥ ring (i.e., $\theta = 0°$) is an ideal configuration for observing such behavior (see Figure 1b). In this configuration, we estimate $\Delta H \approx 8 \times 10^{-9}$ T for ring #1 and $\approx 2 \times 10^{-9}$ T for ring #2. Oscillations with such periods are too small to be detected through our MR(ring, $\theta = 0°$) measurements. The observed oscillations in MR(ring, $\theta = 90°$) may be associated with the AAS effect due to the quantum interference between forward- (weak localization [WL]) and back- (weak antilocalization [WAL]) scattering seen typically in weakly disordered systems with strong spin–orbit coupling.[35–37] Taking the periods of oscillations at 20 K for ring #1 (ΔH(ring #1) ≈ 4.15 T) and ring #2 (ΔH(ring #2) ≈ 3.75 T), we estimate that $S_1 \approx 500$ nm^2 for ring #1 and $S_2 \approx 550$ nm^2 for ring #2. Assuming a circular trajectory, the perimeter for S_1 and S_2 is ≈80–84 nm. This implies that the phase coherence length L_Φ should be comparable with the estimated perimeter. L_Φ can be estimated from the Landauer–Büttiker formula $\Delta G = \frac{e^2/h}{1+L/L_\Phi}$, where ΔG is the oscillation conductance and L is the sample length.[38]. At 20 K, $\Delta G \approx 2.9 \times 10^{-4}(e^2/h)$ for ring #1 and $6.8 \times 10^{-5}(e^2/h)$ for ring #2. The calculated L_Φ(20 K) is 333 nm for ring #1 and 160 nm for ring #2, exceeding the estimated perimeters in ring #1 and ring #2. As plotted in the inset of Figure 3b, L_Φ increases with decreasing T. However, L_Φ does not follow the $T^{-1/2}$ dependence as expected.[35–38]

Even the estimated L_Φ is much longer than the estimated perimeters, we suspect only those circular scattering trajectories more or less normal to the applied field contribute to the oscillation, as H // ring (i.e., $\theta = 90°$). This may explain the absence of the initial sharp rise in MR(ring, $\theta = 90°$), which is one of the characteristics of WAL in the magnetic field. Note that the oscillation in ring #2 is more profound than that in ring #1. This suggests that there are more scattering centers creating more WAL scattering loops in the former case. For ring #1, the relatively large MR at 0.65 K also leads to invisible oscillation.

According to our previous investigation in unbended $TaSe_3$, it requires that $H \approx 100$ T for electrons in the topologically nontrivial α band to reach the first Landau level.[22] Therefore, one would not expect the quantum oscillation beyond the quantum limit under 60 T.[34] However, as discussed above, the electronic structure in the ring-shaped $TaSe_3$ seems severely modified. This may lead to the reduced Fermi velocity and/or enhanced g factor, lowering the critical field for reaching the quantum limit.[34] Given the linear H dependence of both MR(ring, $\theta = 0°$) and MR(ring, $\theta = 90°$) and oscillation above ≈20 T, the inversion of the lowest Landau level beyond the quantum limit may be realized in our ring-shaped samples.

3. Conclusion

In summary, we construct a chain-compound $TaSe_3$ into a ring shape to study the stain effect to the electronic properties. By measuring the magnetotransport of ring-shaped

© 2022 The Authors. Advanced Quantum Technologies published by Wiley-VCH GmbH

25119044, 2022, 12, Downloaded from https://onlinelibrary.wiley.com/doi/10.1002/qute.202200094 by Florida State University, Wiley Online Library on [31/05/2023]. See the Terms and Conditions (https://onlinelibrary.wiley.com/terms-and-conditions) on Wiley Online Library for rules of use; OA articles are governed by the applicable Creative Commons License

samples up to 60 T in both H ⊥ ring ($\theta = 0°$) and H // ring ($\theta = 90°$) configurations, we observe new features that are absent in the unbended (the as-grown shape) samples. One is the violation of the standard Kohler's rule in MR(ring, $\theta = 0°$), which can still be reconciled by introducing temperature-dependent n_T and $n \neq 2$. Upon increasing field to 20 T, n approaches 1, i.e., linear H dependence. At present, it remains unclear whether the linear-H-dependent MR is intrinsic or extrinsic. What is more remarkable is the observation of quantum oscillation in MR(ring, $\theta = 90°$), which can be explained by either the AAS effect involving WAL or the inversion of the lowest Landau level beyond the quantum limit. In either situation, the system must be topologically nontrivial. Our work demonstrates that the shape manipulation of topological materials, particularly with low dimensionality, is an effective way to study novel properties such as WAL and quantum oscillation beyond the quantum limit.

Acknowledgements

This material is based upon work supported by the U.S. Department of Energy under EPSCoR Grant No. DE-SC0012432 and the U.S. National Science Foundation under Grant No. DMR-1504226. A portion of this work was performed at the National High Magnetic Field Laboratory (NHMFL), which was supported by National Science Foundation Cooperative Agreement Nos. DMR-1157490 and DMR- 1644779, the State of Florida and the Department of Energy (DOE). J.S. acknowledges support from the DOE BES program "Science at 100 T," which permitted the design and construction of much of the specialized equipment used in the high-field studies.

Conflict of Interest

The authors declare no conflict of interest.

Data Availability Statement

The data that support the findings of this study are available from the corresponding author upon reasonable request.

Keywords

magnetoresistance, quantum oscillations, strain effect

Received: July 29, 2022
Revised: September 18, 2022
Published online: October 17, 2022

[1] A. A. Soluyanov, D. Gresch, Z. Wang, Q. Wu, M. Troyer, X. Dai, B. A. Bernevig, *Nature* **2015**, *527*, 495.
[2] B. Yan, C. Felser, *Annu. Rev. Condens. Matter Phys.* **2017**, *8*, 337.
[3] T. Liang, Q. Gibson, M. N. Ali, M. Liu, R. J. Cava, N. P. Ong, *Nat. Mater.* **2015**, *14*, 280.
[4] X. Huang, L. Zhao, Y. Long, P. Wang, D. Chen, Z. Yang, H. Liang, M. Xue, H. Weng, Z. Fang, X. Dai, G. Chen, *Phys. Rev. X* **2015**, *5*, 031023.
[5] Y. S. Hor, A. J. Williams, J. G. Checkelsky, P. Roushan, J. Seo, Q. Xu, H. W. Zandbergen, A. Yazdani, N. P. Ong, R. J. Cava, *Phys. Rev. Lett.* **2010**, *104*, 057001.
[6] S. Sasaki, Z. Ren, A. A. Taskin, K. Segawa, L. Fu, Y. Ando, *Phys. Rev. Lett.* **2012**, *109*, 217004.
[7] M. Sato, Y. Ando, *Rep. Prog. Phys.* **2017**, *80*, 076501.
[8] T. Sambongi, M. Yamamoto, K. Tsutsumi, Y. Shiozaki, K. Yamaya, Y. Abe, *J. Phys. Soc. Jpn.* **1977**, *42*, 1421.
[9] M. Yamamoto, *J. Phys. Soc. Jpn.* **1978**, *45*, 431.
[10] S. Nagata, H. Kutsuzawa, S. Ebisu, H. Yamamura, S. Taniguchi, *J. Phys. Chem. Solids* **1989**, *50*, 703.
[11] P. Haen, F. Lapierre, P. Monceau, M. Núnez Regueiro, J. Richard, *Solid State Commun.* **1978**, *26*, 725.
[12] J. Yang, Y. Q. Wang, R. R. Zhang, L. Ma, W. Liu, Z. Qu, L. Zhang, S. L. Zhang, W. Tong, L. Pi, W. K. Zhu, C. J. Zhang, *Appl. Phys. Lett.* **2019**, *115*, 033102.
[13] S. Nie, L. Xing, R. Jin, W. Xie, Z. Wang, F. B. Prinz, *Phys. Rev. B* **2018**, *98*, 125143.
[14] A. Bansil, H. Lin, T. Das, *Rev. Mod. Phys.* **2016**, *88*, 021004.
[15] C. Lin, M. Ochi, R. Noguchi, K. Kuroda, M. Sakoda, A. Nomura, M. Tsubota, P. Zhang, C. Bareille, K. Kurokawa, Y. Arai, K. Kawaguchi, H. Tanaka, K. Yaji, A. Harasawa, M. Hashimoto, D. Lu, S. Shin, R. Arita, S. Tanda, T. Kondo, *Nat. Mater.* **2021**, *20*, 1093.
[16] S. Tanda, T. Tsuneta, Y. Okajima, K. Inagaki, K. Yamaya, N. Hatakenaka, *Nature* **2002**, *417*, 397.
[17] G. Kumagai, T. Matsuura, K. Ichimura, K. Yamaya, K. Inagaki, S. Tanda, *Phys. Rev. B* **2010**, *81*, 184506.
[18] T. Matsuura, K. Inagaki, S. Tanda, *Phys. Rev. B* **2009**, *79*, 014304.
[19] T. Matsuura, T. Tsuneta, K. Inagaki, S. Tanda, *Phys. Rev. B* **2006**, *73*, 165118.
[20] T. Matsuura, T. Tsuneta, G. Kumagai, M. Tsubota, T. Matsuyama, S. Tanda, *Phys. Rev. B* **2011**, *83*, 174113.
[21] Y. Zhang, T. Zhu, H. Bu, Z. Cai, C. Xi, B. Chen, B. Wei, D. Lin, H. Xie, M. Naveed, X. Xi, F. Fei, H. Zhang, F. Song, *AIP Adv.* **2020**, *10*, 095314.
[22] A. I. U. Saleheen, R. Chapai, L. Xing, R. Nepal, D. Gong, X. Gui, W. Xie, D. P. Young, E. W. Plummer, R. Jin, *npj Quantum Mater.* **2020**, *5*, 53.
[23] C. Chen, A. Liang, S. Liu, S. Nie, J. Huang, M. Wang, Y. Li, D. Pei, H. Yang, H. Zheng, Y. Zhang, D. Lu, M. Hashimoto, A. Barinov, C. Jozwiak, A. Bostwick, E. Rotenberg, X. Kou, L. Yang, Y. Guo, Z. Wang, H. Yuan, Z. Liu, Y. Chen, *Matter* **2020**, *3*, 2055.
[24] P. L. Cai, J. Hu, L. P. He, J. Pan, X. C. Hong, Z. Zhang, J. Zhang, J. Wei, Z. Q. Mao, S. Y. Li, *Phys. Rev. Lett.* **2015**, *115*, 057202.
[25] J. Xu, F. Han, T.-T. Wang, L. R. Thoutam, S. E. Pate, M. Li, X. Zhang, Y.-L. Wang, R. Fotovat, U. Welp, X. Zhou, W.-K. Kwok, D. Y. Chung, M. G. Kanatzidis, Z.-L. Xiao, *Phys. Rev. X* **2021**, *11*, 041029.
[26] A. A. Abrikosov, *Phys. Rev. B* **1998**, *58*, 2788.
[27] R. A. Young, *Phys. Rev.* **1968**, *175*, 813.
[28] A. A Abrikosov, *Europhys. Lett.* **2000**, *49*, 789.
[29] R. A. Young, *Phys. Rev.* **1968**, *175*, 813.
[30] J. C. W. Song, G. Refael, P. A. Lee, *Phys. Rev. B* **2015**, *92*, 180204.
[31] R. Xu, A. Husmann, T. F. Rosenbaum, M.-L. Saboungi, J. E. Enderby, P. B. Littlewood, *Nature* **1997**, *390*, 57.
[32] Y. Aharonov, D. Bohm, *Phys. Rev.* **1959**, *115*, 485.
[33] B. L. Al'Tshuler, A. G. Aronov, B. Z. Spivak, *JETP Lett.* **1981**, *33*, 94.
[34] C. M. Wang, H.-Z. Lu, X. C. Xie, *Phys. Rev. B* **2020**, *102*, 041204(R).
[35] J. Chen, H. J. Qin, F. Yang, J. Liu, T. Guan, F. M. Qu, G. H. Zhang, J. R. Shi, X. C. Xie, C. L. Yang, K. H. Wu, Y. Q. Li, L. Lu, *Phys. Rev. Lett.* **2010**, *105*, 176602.
[36] H.-T. He, G. Wang, T. Zhang, I.-K. Sou, G. K. L Wong, J.-N. Wang, H.-Z. Lu, S.-Q. Shen, F.-C. Zhang, *Phys. Rev. Lett.* **2011**, *106*, 166805.
[37] K. Shrestha, M. Chou, D. Graf, H. D. Yang, B. Lorenz, C. W. Chu, *Phys. Rev. B* **2017**, *95*, 195113.
[38] G. Fagas, J. C. Greer, *Nano Lett.* **2009**, *9*, 1856.

© 2022 The Authors. Advanced Quantum Technologies published by Wiley-VCH GmbH

25119044, 2022, 12, Downloaded from https://onlinelibrary.wiley.com/doi/10.1002/qute.202200094 by Florida State University, Wiley Online Library on [31/05/2023]. See the Terms and Conditions (https://onlinelibrary.wiley.com/terms-and-conditions) on Wiley Online Library for rules of use; OA articles are governed by the applicable Creative Commons License